COMPENSATION OF TIME-VARYING HARMONIC DISTURBANCES ON NONLINEAR BEARINGLESS SLICE MOTORS

Christian Hüttner [*], **Jochen M. Rieber** [*], **Frank Allgöwer** [*,1], **Jörg Hugel** [**]

[*] *Institute for Systems Theory in Engineering, University of Stuttgart, Pfaffenwaldring 9, 70550 Stuttgart, Germany*

[**] *Electrical Engineering and Design Laboratory, Swiss Federal Institute of Technology Zurich, 8005 Zurich, Switzerland*

Abstract: The rotor position of magnetic bearings or bearingless slice motors is usually subject to several harmonic disturbances with time-varying frequencies. To achieve low power consumption and good vibration suppression, efficient control algorithms have to be invoked. In this contribution, exact input-output linearization is applied to a nonlinear bearing model, followed by output regulation via the internal model principle. The resulting disturbance rejection approach does not need to know the disturbance amplitude and phase, and changes its behavior according to the measured disturbance frequency. The method is tested in simulations related to a prototype magnetic bearing.

Keywords: Magnetic bearings, vibration suppression, nonlinear systems, exact input-output linearization, output regulation.

1. INTRODUCTION

Magnetic bearings or bearingless slice motors are used in a wide variety of applications like low-friction drive systems or left ventricular assist devices (LVAD) (see Figure 1). The occurrence of undesired harmonic disturbances in such magnetic bearings is common. Usually the reason is a divergence between the rotational axis and the axis of inertia such that unbalance is the result. The unbalance applies harmonic disturbance in the rotational frequency. While the first harmonic of such a disturbance is caused by unbalance, higher harmonics occur and are due to asymmetries in the motor flux. The disturbance frequencies are known via measurement. However, these frequencies are not constant which makes the system parameter time-varying.

There are numerous works published, e.g. early ones (Burrows and Sahinkaya, 1983; Burrows and Sahinkaya, 1989), which were extended by (Knospe, 1991; Knospe and Tamer, 1996; Knospe et al., 1997). Some approaches propose the insertion of a notch filter into the control loop (Herzog et al., 1996), which might cause problems since the transfer function is modified.

In this work a bearingless slice motor is considered. Additionally to the fundamental harmonic disturbance frequency due to unbalance, also higher harmonic disturbances, mainly in the second harmonic frequency exist. In (Huettner, 2003), an open-loop algorithm for the compensation of several harmonics is presented. Since four harmonics are considered, the computational modification proposed there caused an increase in convergence time. However, the method is robust such that no further modeling of the vibrations' source is necessary.

[1] Corresponding author: F. Allgöwer.
Email: allgower@ist.uni-stuttgart.de

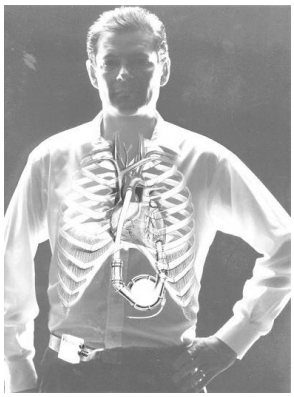

Fig. 1. Implant of an LVAD at the example of HeartMate-I (courtesy of Thoratec Inc.)

The goal of the presented strategy in this paper is to provide a closed controller and disturbance rejection design to satisfy all regulation needs for the considered bearing. First, the system is exactly input-output linearized. Second, output regulation based on the internal model principle is applied to reject the disturbances. The internal model is designed such that several harmonic disturbances are compensated simultaneously. This results in a controller easily tunable under physical considerations. Furthermore, the internal model considers the varying disturbance frequency and leads to a parameter-varying controller. Finally, reduced-order observers are applied to prevent unnecessary estimates of measurable signals.

Further internal model controller designs for magnetic levitation systems are found in (Alleyne and Pomykalski, 2000), where a single degree-of-freedom (SDOF) ball system with constant disturbance frequency is considered. Disturbance compensation is simulated in (Gentili and Marconi, 2002) for another SDOF levitation system, and realized for a suspension stage in (Shan and Menq, 2002).

2. MODEL AND LINEARIZATION

2.1 Bearing Model

Figure 2 displays the setup of the bearingless slice motor. The so called "temple design" is chosen due to easier pump head design for industrial applications. For simplicity, two separate coil circuits exist, the lower one for the drive and the upper one to provide the magnetic bearing. The rotor is a 2-pole permanent magnet. The coordinate setup used for the equations is shown in Figure 3.

A mathematical model of the bearingless slice motor (see Table 1 for an explanation of symbols) is based upon the choice

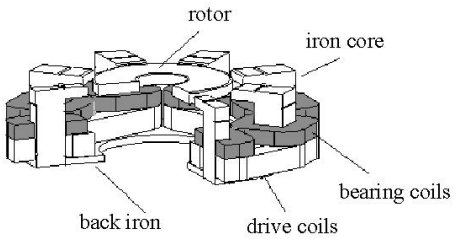

Fig. 2. Temple motor.

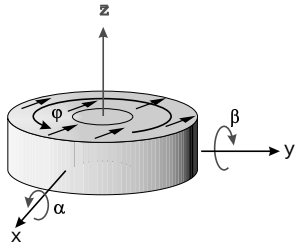

Fig. 3. Coordinate system of the disc.

$$\begin{aligned}\boldsymbol{u} &= [u_x,\, u_y,\, u_m]^T \\ \boldsymbol{x} &= [i_x,\, i_y,\, i_m,\, x,\, y,\, \varphi,\, v_x,\, v_y,\, \omega]^T \\ \boldsymbol{y} &= [x,\, y,\, \varphi]^T\end{aligned}$$

of control variables $\boldsymbol{u}$, states $\boldsymbol{x}$, and measurement outputs $\boldsymbol{y}$. First-principles modeling results in the nonlinear differential equations (Huettner, 2003)

$$\begin{aligned}\dot{\boldsymbol{x}} &= \boldsymbol{f}(\boldsymbol{x}) + \boldsymbol{b}\boldsymbol{u} \\ \boldsymbol{y} &= \boldsymbol{H}\boldsymbol{x},\end{aligned} \tag{1}$$

where

$$\boldsymbol{f}(\boldsymbol{x}) = \begin{bmatrix} -\frac{R}{L}\begin{bmatrix} i_x \\ i_y \end{bmatrix} - \frac{k_i}{L}\begin{bmatrix} v_x \\ v_y \end{bmatrix} \\ -\frac{R_A}{L_A} i_m \\ v_x \\ v_y \\ \omega \\ \frac{k_i}{m}\begin{bmatrix} i_x \\ i_y \end{bmatrix} + \frac{k_s}{m}\left(\boldsymbol{I}_2 + c_s \boldsymbol{C}_2\right)\begin{bmatrix} x \\ y \end{bmatrix} \\ \frac{m}{2}\Psi_{PM} i_m \end{bmatrix} \tag{2}$$

$$\boldsymbol{b} = \begin{bmatrix} \frac{1}{L} & 0 & 0 \\ 0 & \frac{1}{L} & 0 \\ 0 & 0 & \frac{1}{L_A} \\ \boldsymbol{0}_{6,1} & \boldsymbol{0}_{6,1} & \boldsymbol{0}_{6,1} \end{bmatrix} \tag{3}$$

$$\boldsymbol{H} = [\,\boldsymbol{0}_{3,3} \quad \boldsymbol{I}_3 \quad \boldsymbol{0}_{3,3}\,] \tag{4}$$

$$\boldsymbol{C}_2 = \begin{bmatrix} \cos(2\varphi) & \sin(2\varphi) \\ \sin(2\varphi) & -\cos(2\varphi) \end{bmatrix}. \tag{5}$$

The model of the bearing is also shown in block diagram form in Figure 4. There the matrix block $\boldsymbol{C}_s = k_s(\boldsymbol{I}_2 + c_s\boldsymbol{C}_2)$ combines the force-position feedback factor k_s as well as the coupling matrix $\boldsymbol{C}_2$. The matrix block $\boldsymbol{C_i} = k_i\boldsymbol{I}_2$ represents the force-current factor k_i in this simplified case.

Table 1. Symbols of the bearing model.

Symbol	Description
u_x, u_y, u_m	coil circuit voltages
i_x, i_y, i_m	coil currents
x, y	rotor center position
v_x, v_y	rotor center velocities
φ	rotor angle
ω	rotor angular velocity
R	bearing coil resistance
L	bearing coil inductivity
R_A	drive coil resistance
L_A	drive coil inductivity
k_i	force - current factor
k_s	force - position factor
c_s	coupling constant
m	rotor mass
Ψ_{PM}	rotor flux
$\boldsymbol{I}_n$	n-dimensional identity matrix
$\boldsymbol{0}_{m,n}$	$m \times n$-dimensional zero matrix

The rotor is modeled as a thin disc. Its dynamics corresponding to the passively stabilized degrees of freedom ($\alpha = 0$, $\beta = 0$, $z = 0$, see Figure 3) are not considered, since only small deviations are assumed. Hence in the model only the translatory motion in the x-y plane and the rotatory motion around the z-axis are modeled. This simplification is tolerable because the system is driven at relatively low speeds. According to (Leier, 1999), where Leier discusses nonlinearities in magnetic bearings, the force-distance factor and therefore the coupling by means of $\boldsymbol{C}_s$ has the most influence. This is especially true when considering a magnetic sphere, where in fact only half a degree of freedom can be controlled (the other half would be gravity). In magnetic bearings, two opposite coils acting in the same degree of freedom practically ensure linearity around the operational point by superposing their force-current, force-position characteristics. In the described bearingless slice motor, the nonlinearity introduced by $c_s\boldsymbol{C}_2$ has far more influence (c_s may reach up to 0.5) and therefore all other nonlinearities are neglected.

2.2 Exact Input-Output Linearization

Exact input-output linearization has been used for various magnetic bearings (e.g. see (Namerikawa et al., 1998; Lindlau and Knospe, 2000)) mainly to linearize the force-position, force-current relation.

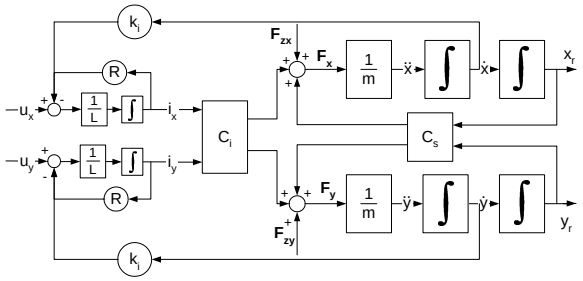

Fig. 4. Schematic model of the magnetic bearing.

Applying the standard procedure of exact input-output linearization (for further reading see e.g. (Isidori, 1995; Khalil, 2002)) to the considered equations yields a linear and decoupled system.

With the nonlinear feedback law

$$\boldsymbol{u} = \boldsymbol{\alpha}(\boldsymbol{x}) + \boldsymbol{\nu} = \begin{bmatrix} \alpha_x(\boldsymbol{x}) \\ \alpha_y(\boldsymbol{x}) \\ 0 \end{bmatrix} + \begin{bmatrix} \nu_x \\ \nu_y \\ \nu_m \end{bmatrix}, \quad (6)$$

where

$$\begin{aligned} \alpha_x(\boldsymbol{x}) =& \frac{R}{i_x} + k_i v_x - L\frac{k_s}{k_i}(1 + c_s\cos(2\varphi))v_x \\ & - L\frac{k_s}{k_i}c_s\sin(2\varphi)\,v_y \\ & + 2L\frac{k_s}{k_i}c_s(x\sin(2\varphi) - y\cos(2\varphi))\omega \\ \alpha_y(\boldsymbol{x}) =& \frac{R}{i_y} + k_i v_y - L\frac{k_s}{k_i}(1 - c_s\cos(2\varphi))v_y \\ & - L\frac{k_s}{k_i}c_s\sin(2\varphi)\,v_x \\ & - 2L\frac{k_s}{k_i}c_s(y\sin(2\varphi) + x\cos(2\varphi))\omega, \end{aligned}$$

the transformed system dynamics for each axis [2] emerge to

$$\dot{\boldsymbol{z}} = \boldsymbol{A}\boldsymbol{z} + \boldsymbol{B}\nu \quad (7)$$

$$\boldsymbol{y} = \boldsymbol{C}\boldsymbol{z} \quad (8)$$

with

$$\boldsymbol{A} = \begin{bmatrix} 0 & 0 & 1 \\ 0 & 0 & 0 \\ 0 & 1 & 0 \end{bmatrix}, \quad \boldsymbol{B} = \begin{bmatrix} 0 \\ 1 \\ 0 \end{bmatrix}, \quad \boldsymbol{C} = \begin{bmatrix} 1 \\ 0 \\ 0 \end{bmatrix}^T \quad (9)$$

in the new state variables $\boldsymbol{z}$ being equal to either $\boldsymbol{z}_x$ or $\boldsymbol{z}_y$, and the new system input ν being equal to either ν_x or ν_y. The transformation is described by

$$\boldsymbol{z} = \begin{bmatrix} \boldsymbol{z}_x \\ \boldsymbol{z}_y \\ \boldsymbol{z}_m \end{bmatrix} = \boldsymbol{T}(\boldsymbol{x}) \quad (10)$$

$$= \begin{bmatrix} x \\ v_x \\ \frac{k_i}{m}i_x + \frac{k_s}{m}\left(x\left(1 + c_s\cos(2\varphi)\right) + yc_s\sin(2\varphi)\right) \\ y \\ v_y \\ \frac{k_i}{m}i_y + \frac{k_s}{m}\left(y\left(1 - c_s\cos(2\varphi)\right) + xc_s\sin(2\varphi)\right) \\ \varphi \\ \omega \\ \frac{m}{2}\Psi_{PM}i_m \end{bmatrix}. \quad (11)$$

The well-defined vector relative degree of the system is $\{3, 3, 3\}$, there are no zero dynamics, and the system is nonlinear minimum phase. Now both axes can be considered equal and independent, which reduces the number of states for controller design to three for each axis.

[2] The linear drive model (states i_m, φ, ω) is not further considered. Its states influence the linearizing equations.

3. OUTPUT REGULATION

3.1 Error Feedback Design

To the linearized system equations (7)–(8), output regulation using an internal model is applied. The reader is referred to (Knobloch et al., 1993) for details.

The coil currents i_x, i_y and the rotor-center positions x, y of the bearingless slice motor are measured states, whereas the transient velocities are not available. Since full information is not provided, a design for error feedback is used. The design model for each axis follows from (7)–(8), augmented with the disturbance inputs, as

$$\dot{\boldsymbol{z}} = \boldsymbol{A}\boldsymbol{z} + \boldsymbol{B}\nu + \boldsymbol{P}\boldsymbol{w} \tag{12}$$

$$e = \boldsymbol{C}\boldsymbol{z} + \boldsymbol{Q}\boldsymbol{w}\,. \tag{13}$$

Since unbalance can be described as a mass being positioned at a given eccentricity, it is best modeled by an additional contribution to the accelerations resulting in:

$$\boldsymbol{P} = \begin{bmatrix} 0 & 0 & 0 \\ 0 & 0 & 0 \\ 1 & 1 & 1 \end{bmatrix}, \quad \boldsymbol{Q} = \begin{bmatrix} 0 \\ 0 \\ 0 \end{bmatrix}^T. \tag{14}$$

The disturbance signal is assumed to be generated by the anti-stable exosystem $\dot{\boldsymbol{w}} = \boldsymbol{S}\boldsymbol{w}$ with

$$\boldsymbol{S} = \begin{bmatrix} 0 & -\omega & 0 \\ \omega & 0 & 0 \\ 0 & 0 & 0 \end{bmatrix}, \tag{15}$$

which results in a disturbance $\boldsymbol{P}\boldsymbol{w} = \bar{A}_0 + \bar{A}\sin(\omega t + \phi)$, i.e. a constant superposed by a sine wave. Note that an integrator is included into the disturbance model. An influence in the position sensors, caused by the relatively strong field of the permanent magnetic rotor, might require a modified $\boldsymbol{P}$ as well as a harmonic disturbance in the current signal which cannot be modeled as direct influence on a state z. Combinations of disturbances caused numerical instabilities.

For each axis, an error-feedback controller is sought, guaranteeing closed-loop stability and an asymptotically vanishing control error e. Assuming stabilizability of the pair $(\boldsymbol{A}, \boldsymbol{B})$ and detectability of

$$\left(\begin{bmatrix} \boldsymbol{C} & \boldsymbol{Q} \end{bmatrix}, \begin{bmatrix} \boldsymbol{A} & \boldsymbol{P} \\ \boldsymbol{0} & \boldsymbol{S} \end{bmatrix} \right), \tag{16}$$

it can be shown (Knobloch et al., 1993), that a controller of the form

$$\begin{bmatrix} \dot{\boldsymbol{\xi}}_0 \\ \dot{\boldsymbol{\xi}}_1 \end{bmatrix} = \begin{bmatrix} \boldsymbol{A} - \boldsymbol{G}_0\boldsymbol{C} + \boldsymbol{B}\boldsymbol{K} & \boldsymbol{P} - \boldsymbol{G}_0\boldsymbol{Q} + \boldsymbol{B}(\boldsymbol{\Gamma} - \boldsymbol{K}\boldsymbol{\Pi}) \\ -\boldsymbol{G}_1\boldsymbol{C} & \boldsymbol{S} - \boldsymbol{G}_1\boldsymbol{Q} \end{bmatrix} \begin{bmatrix} \boldsymbol{\xi}_0 \\ \boldsymbol{\xi}_1 \end{bmatrix} + \begin{bmatrix} \boldsymbol{G}_0 \\ \boldsymbol{G}_1 \end{bmatrix} e \tag{17}$$

$$\nu = \begin{bmatrix} \boldsymbol{K} & (\boldsymbol{\Gamma} - \boldsymbol{K}\boldsymbol{\Pi}) \end{bmatrix} \begin{bmatrix} \boldsymbol{\xi}_0 \\ \boldsymbol{\xi}_1 \end{bmatrix} \tag{18}$$

satisfies the requirements if and only if $\boldsymbol{\Pi}$, $\boldsymbol{\Gamma}$ are found such that

$$\boldsymbol{\Pi}\boldsymbol{S} = \boldsymbol{A}\boldsymbol{\Pi} + \boldsymbol{B}\boldsymbol{\Gamma} + \boldsymbol{P} \tag{19}$$

$$\boldsymbol{0} = \boldsymbol{C}\boldsymbol{\Pi} + \boldsymbol{Q} \tag{20}$$

hold and $\boldsymbol{K}$, $\boldsymbol{G}_0$, $\boldsymbol{G}_1$ are chosen such that the matrices

$$\boldsymbol{A} + \boldsymbol{B}\boldsymbol{K} \quad \text{and} \quad \begin{bmatrix} \boldsymbol{A} & \boldsymbol{P} \\ \boldsymbol{0} & \boldsymbol{S} \end{bmatrix} - \begin{bmatrix} \boldsymbol{G}_0 \\ \boldsymbol{G}_1 \end{bmatrix} \begin{bmatrix} \boldsymbol{C} & \boldsymbol{Q} \end{bmatrix} \tag{21}$$

are asymptotically stable. This setup guarantees that a model of the exosystem is included in the controller. For proofs and further details the reader is referred to (Francis and Wonham, 1976; Knobloch et al., 1993).

3.2 Multiple Harmonics

A fourier analysis of the position or current signals shows the necessity to also compensate higher harmonic frequencies. In some cases, the second harmonic contains more saveable energy than the first one (Huettner, 2003). Since the considered nonlinearity factor c_s disturbs the bearing with the period of π, the expected amount of energy to be saved by suppressing the second harmonic decreases with exact linearization. Depending on the size of the motor and the operating conditions of the pump, higher harmonics show varying contributions and therefore varying energy saving potential. In practical cases between two (1st and 2nd) and four (1st...4th) harmonics need to be compensated simultaneously. Extending the internal model to higher harmonics requires the matrices $\boldsymbol{P_{mH}}$, $\boldsymbol{Q_{mH}}$ and $\boldsymbol{S_{mH}}$ to model the extended exosystem instead of $\boldsymbol{P}$, $\boldsymbol{Q}$, and $\boldsymbol{S}$:

$$\boldsymbol{P_{mH}} = \begin{bmatrix} 0 & 0 & 0 & 0 & \dots & 0 \\ 0 & 0 & 0 & 0 & \dots & 0 \\ 1 & 1 & 1 & 1 & \dots & 1 \end{bmatrix}, \qquad \boldsymbol{Q_{mH}} = \begin{bmatrix} 0 \\ \vdots \\ 0 \end{bmatrix}^T$$

$$\boldsymbol{S_{mH}} = \begin{bmatrix} 0 & -\omega & 0 & 0 & \dots & 0 \\ \omega & 0 & 0 & 0 & \dots & 0 \\ 0 & 0 & 0 & -2\omega & \dots & 0 \\ 0 & 0 & 2\omega & 0 & \dots & 0 \\ \vdots & \vdots & \vdots & \vdots & \ddots & 0 \\ 0 & 0 & 0 & 0 & 0 & 0 \end{bmatrix}.$$

4. CONTROLLER DESIGN

4.1 State Controller

The design of the state controller $\boldsymbol{K}$ is straightforward using pole placement. Since the physical relation to two states per axis is still given after linearization, a manual tuning on the product is still possible to compensate modeling errors.

4.2 Frequency Variation

Due to the applications of the considered bearingless slice motors, the range of possible rotational speeds is limited by $\omega \in [\omega_{min} \dots \omega_{max}]$. In this application, a technique similar to the one in (Francis and Vidyasagar, 1978) is used. There the internal model controller depends on

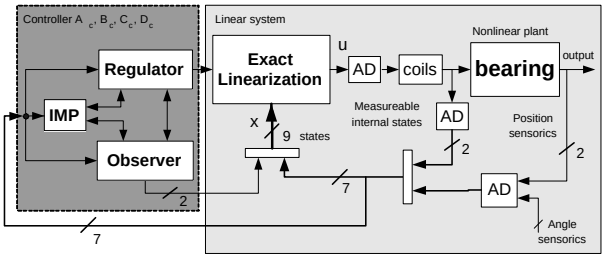

Fig. 5. E/A-liearized magnetic bearing with IMP regulator and reduced-order observer.

the time-varying parameters of $\boldsymbol{S}$, and an adaptive observer estimates the true values of these parameters. However, the frequencies ω can be measured directly in this application, which makes the estimator superfluous. Practical frequency variations have to be much slower than observer convergence time. The suppression of the harmonic disturbances has to be independent of small frequency variations, e.g. measurement noise.

4.3 Linear Reduced Observer

Since two states per axis (currents and positions) can be measured, the full observer in equation (17) is not necessary and can be reduced to the order $2 + 2n$ (n being the number of harmonics to be compensated). Basics on reduced-order observers can be found in (Friedland, 1996). Considering the case for one harmonic, the (6×6) matrix $\boldsymbol{A}_{imp}(\omega)$, which is the dynamic matrix of the system augmented by the dynamics of the internal model, can be split into the measurable part $\boldsymbol{A}_{imp_{1..2,1..2}}$ and a part which has to be observed. The observer design is now reduced to finding a $\boldsymbol{G}_R(\omega)$, such that $(\boldsymbol{A}_{imp_{3..6,3..6}}(\omega) - \boldsymbol{G}_R(\omega)\boldsymbol{A}_{imp_{1..2,3..6}})$ is Hurwitz (for ω_R). This is done by pole placement, with frequency-invariant poles. The combination of the extended state controller $\boldsymbol{K}_{imp}$ and the observer (for one axis) gives:

$$
\begin{aligned}
\boldsymbol{K}_{imp}(\omega) &= \begin{bmatrix}\boldsymbol{K} & \boldsymbol{\Gamma}(\omega) - \boldsymbol{K}\boldsymbol{\Pi}\end{bmatrix} \\
\boldsymbol{A}_c(\omega) &= \boldsymbol{A}_{imp_{3..6,3..6}}(\omega) - \boldsymbol{G}_R(\omega)\boldsymbol{A}_{imp_{1..2,3..6}} \\
\boldsymbol{B}_c(\omega) &= \boldsymbol{A}_{imp_{3..6,1..2}} - \boldsymbol{G}_R(\omega)\boldsymbol{A}_{imp_{1..2,1..2}} \\
&\quad + \boldsymbol{A}_c(\omega)\boldsymbol{G}_R(\omega) \\
\boldsymbol{C}_c(\omega) &= \boldsymbol{K}_{imp_{3..6}}(\omega) \\
\boldsymbol{D}_c(\omega) &= \boldsymbol{K}_{imp_{1..2}} + \boldsymbol{K}_{imp_{3..6}}(\omega)\boldsymbol{G}_R(\omega).
\end{aligned}
$$

The controller including the state controller, internal model principle part and reduced observer is now given by $\boldsymbol{A}_c$, $\boldsymbol{B}_c$, $\boldsymbol{C}_c$, $\boldsymbol{D}_c$. The embedding of the controller in the linearized plant is shown in figure 5.

5. RESULTS

The solution of the regulator equations for the chosen disturbance model (14)–(15) and the linearized model (7)–(8) are the matrices $\boldsymbol{\Pi}$, $\boldsymbol{\Gamma}$ and $\boldsymbol{G}_R$:

$$
\boldsymbol{\Pi} = \begin{bmatrix} 0 & 0 & 0 \\ -1 & -1 & -1 \\ 0 & 0 & 0 \end{bmatrix}, \boldsymbol{\Gamma} = \begin{bmatrix} -\omega \\ \omega \\ 0 \end{bmatrix}^T, \boldsymbol{G_R} = \begin{bmatrix} g_{r,11} & 0 \\ g_{r,21} & 0 \\ g_{r,31} & 0 \\ g_{r,41} & 0 \end{bmatrix}.
$$

The components of $\boldsymbol{G}_R$ (where p_i are observer poles) emerge to:

$$
\begin{aligned}
g_{r,11} &= -p_1 - p_2 - p_3 - p_4 \\
g_{r,\binom{2}{3}1} &= \frac{1}{2}\Big(-\omega^2 + p_3p_4 + p_2p_4 + p_2p_3 + p_1p_2 \\
&\quad + p_1p_3 + p_1p_4 - g_{r,41} \mp g_{r,11}\omega \\
&\quad \pm \frac{1}{\omega}(p_1p_2p_3 + p_1p_2p_4 + p_1p_3p_4 + p_2p_3p_4)\Big) \\
g_{r,41} &= \frac{p_1p_2p_3p_4}{\omega^2}.
\end{aligned}
$$

In the main target application, the LVAD (see figure 1) , the pump is working in parallel to a human heart. During one heartbeat-cycle (1.2 Hz), the rotational speed of the pump changes because of pump-pressure and resistance interactions. The frequency variation of this modulated signal is up to 7 Hz. Therefore fast but small speed variations have to be tolerated.

Figure 6 shows the normalized x-position signal for varying frequencies but constant amplitudes in the upper plot for ideal simulation setup. The corresponding normalized disturbance amplitude and frequency is shown in the lower plot. The controller copes with the modeled harmonic disturbances. The varying controller parameters capture the varying disturbance frequency. At $t = 0.26$ s, the designed output regulator is switched off, leading to a significantly disturbed position signal.

In Figure 7, the location of the disturbance influence is varied for a constant disturbance frequency and amplitude. First, for $t \in [0.03, 0.1]$ s, the disturbance acts on the current signal. Second, a force disturbance as designed is applied for $t \in [0.1, 0.2]$ s. Finally, an output disturbance is assumed for $t \in [0.2, 0.3]$ s. The controller suppresses all three kinds of disturbance influences reasonably well, although it was only designed for force (acceleration) disturbances.

6. CONCLUSIONS

In this paper, the application of the internal model principle for asymptotic rejection of harmonic disturbances in bearingless slice motors is examined. Output regulation using exact input-output linearization, an internal model compensator and

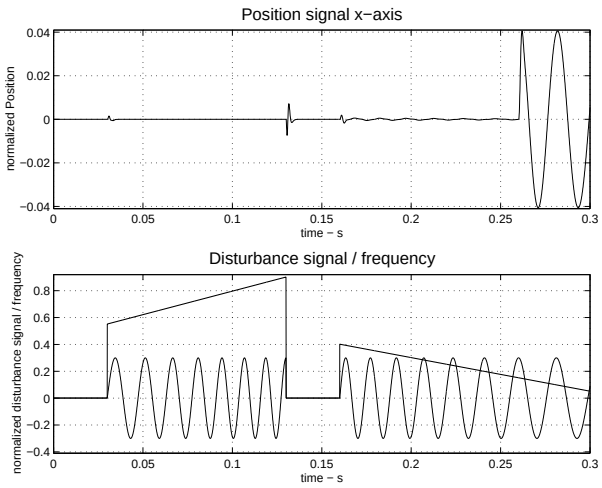

Fig. 6. Position with a varying disturbance frequency.

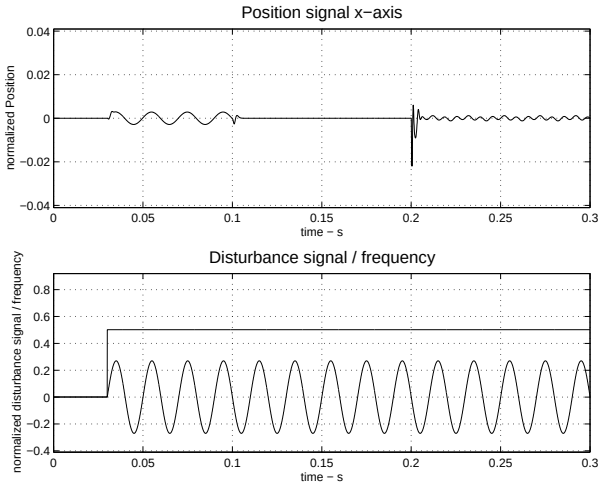

Fig. 7. Position with a varying disturbance influence location.

a reduced-order observer is integrated into an parameter-varying nonlinear controller. Knowledge on the disturbance magnitude and phase is not required, whereas its frequency is directly measured and used as a controller parameter. The presented vibration control strategy shows excellent simulation performance and promises to be efficiently usable in future prototype experiments.

The implementation on a DSP is straightforward for a fixed rotational frequency. Due to the parameter variation caused by the disturbance frequency change, a symbolic discretization is necessary. The resulting parameters are up to 6th-order polynomials in the frequency which demands too much online computation power. To keep the controller evaluation time down to a reasonable amount, simple look-up tables have to be implemented, where not all parameters depend on the frequency. In that way the compensation of higher order harmonics requires little additional implementation effort and computation power.

ACKNOWLEDGEMENTS

The authors want to thank the company Levitronix LLC for providing their latest product hardware and for offering the environment to investigate on different bearingless slice motors.

REFERENCES

Alleyne, A. and M. Pomykalski (2000). Control of a Class of Nonlinear Systems Subject to Periodic Exogenous Signals. *IEEE Trans. Control Systems Technology*, **8**(2), 279–287.

Burrows, C.R. and M.N. Sahinkaya (1983). Vibration Control of Multimode Rotor-Bearing Systems. *Proc. Royal Society of London A*, **386**.

Burrows, C.R. and M.N. Sahinkaya (1989). Active Vibration Control of Flexible Rotors: An Experimental and Theoretical Study. *Proc. Royal Society of London A*, **422**.

Francis, B.A. and M. Vidyasagar (1978). Adaptive robust regulation of linear multivariable systems. *Proc. IEEE Conf. Decision and Control*, pp. 1098–1100.

Francis, B.A. and W.M. Wonham (1976). The Internal Model Principle of Control Theory. *Automatica*, **12**(5), 457–465.

Friedland, B. (1996). Observers. In: *The Control Handbook*, CRC Press.

Gentili, L. and L. Marconi (2003). Robust Nonlinear Disturbance Suppression of a Magnetic Levitation System. *Automatica*, **39**(4), 735–742.

Herzog, R., P. Buehler, C. Gaehler and R. Larsonneur (1996). Unbalance Compensation using Generalized Notch Filters in the Multivariable Feedback of Magnetic Bearings. *IEEE Trans. Control Systems Technology*, **4**(5).

Huettner, C. (2003). *Regelungskonzepte magnetisch gelagerter Scheibenmotoren (German)*. Dissertation ETH Zurich Nr. 15092, Zurich, Switzerland.

Isidori, A. (1995). *Nonlinear Control Systems*, Springer, New York, USA.

Khalil, H.K. (2002). *Nonlinear Systems*, Third Edition, Prentice Hall, Upper Saddle River, NJ, USA.

Knobloch, H.-W., A. Isidori and D. Flockerzi (1993). *Topics in Control Theory*, Birkhaeuser, Basel, Switzerland.

Knospe, C. (1991) Stability and Performance of Notch Filter Controllers for Unbalance Response. *Int. Symp. Magnetic Suspension Technology*, NASA Conf. Pub. 3152, Hampton, VA, USA.

Knospe, C. and S. Tamer (1996). Experiments in Robust Unbalance Control. *5th Int. Symp. Magnetic Bearings*, Kanazawa, Japan.

Knospe, C., S. Tamer and R. Fittro (1997). Rotor Synchronous Response Control: Approaches for Addressing Speed Dependence. *Journal of Vibration and Control*, **3**.

Leier, D. (1999). *Nichtlinearitaeten magnetgelagerter Rotorsysteme (German)*, Springer, Berlin, Germany.

Lindlau, J.D. and C.R. Knospe (2000). High Performance Voltage Control using Feedback Linearization. *7th Int. Symp. Magnetic Bearings*, Zurich, Switzerland.

Namerikawa, T., M. Fujita and F. Matsumura (1998). Wide Area Stabilization of a Magnetic Bearing using Exact Linearization. *6th Int. Symp. Magnetic Bearings*, Cambridge, USA.

Shan, X. and C.-H. Menq (2002). Robust Disturbance Rejection for Improved Dynamic Stiffness of a Magnetic Suspension Stage. *IEEE/ASME Trans. Mechatronics*, **7**(3).